SAE International

Aerodynamic Investigation on the Effect of Varying Through-Hub Flow on a Formula One Front Wheel Assembly

2011-01-1431
Published
04/12/2011

A. J. Sprot, J. B. Minto, D. B. Sims-Williams and R. G. Dominy
Durham University

doi:10.4271/2011-01-1431

ABSTRACT

For open wheel race cars the front wheel flow and the interaction of its wake with downstream components is of significant importance. Considerable effort goes into the design of front wing end plates, barge boards and underfloor components in order to manage the front wheel flow. In this study a 50% scale Formula One front wheel assembly has been tested in the Durham University $2m^2$ open jet wind tunnel to evaluate the effect of through-hub flow on its cooling drag and flow structures. Varying the amount of through-hub flow gave rise to a negative cooling drag trend whereby increasing the flow through the hub resulted in a decrease in drag.

This observation has been explained both qualitatively and quantitatively by inlet spillage drag. Lower than optimum airflows through the brake scoop result in undesirable separation at the inside edge and hence, an increase in drag (reversing the cooling drag trend). The dominant processes at different flow rates have been assessed by applying several modifications to the scoop design in order to suppress or overcome the contributions to the drag change. This methodology has also shown a greater aerodynamic efficiency across the whole through-hub flow range for the case with rounded edges.

A combination of PIV, pressure probe wake maps, CFD and surface flow visualisation techniques have been used to investigate the effect of through-hub flow on the overall wake of the wheel. The well documented counter rotating vortices or ground lobes are shown to be displaced toward the outboard side due to the outflow of the cooling flow causing a lower pressure. The size of these vortices also changes significantly with through-hub flow rate. The effect of outboard wheel fairings has been investigated in the context of through-hub flow. By positioning the exit orifice facing downward or rearward, the overall drag was significantly reduced and the structure of the wake was further altered toward the outboard side.

INTRODUCTION

OPEN WHEEL AERODYNAMICS

Isolated and exposed wheel flows have been a subject of investigation for decades due to their influence on the overall vehicle flow field. However, the complexity in recording data from a rotating object has resulted in relatively slow progress in our understanding. It has been reported that the exposed rotating wheels of a grand prix car contribute between 35 and 50 percent of the overall drag of the vehicle (Dominy [1]). The downstream wake structure and flow field around the front wheels are significant as the majority of the car is affected by these. Formula One (F1) aerodynamicists spend a considerable amount of time redirecting the flow upstream and downstream of the front wheels in order to achieve a suitable airflow for downstream components such as the side pods and rear wing. Front wing end plates, barge boards and underfloor components are examples of devices used to achieve this. The technical regulations of racing formulae such as F1 dictate that the wheels must not be enclosed. Recently, further restrictions have been put in place, such as banning outboard wheel fairings, further curtailing how an aerodynamicist can control the flow field of the wheel.

One of the earliest fundamental studies of rotating wheel flows in isolation was conducted by Fackrell and Harvey [2-3] (more depth in Fackrell [4]). The study established

positive lift and drag which are characteristic of a wheel in ground contact and demonstrated how both quantities reduce with rotation due to the forward movement of the separation point. Due to the varying ground reaction force experienced by a rotating wheel, lift measurement becomes problematic as separating the mechanical from aerodynamic forces is unreliable.

Morelli [5] attempted to overcome this by raising the wheel off the floor. This method highlights the necessity to maintain full ground contact at all times as this led to negative lift conclusions. The reason for this downforce was due to the accelerating airflow under the tyre which caused a low pressure region. Stapleford and Carr [6] used a similar method but blocked the gap with strips of paper to prevent the negative lift measurement problem.

Generally, the accepted method of testing a wheel in a wind tunnel comprises a moving ground plane with the wheel in full contact across its full width. Mears et al. [7,8,9] used a radio telemetry system to measure surface static pressure at different locations on the tyre's tread. This resulted in confirming Fackrell's summary of the aerodynamics of a rotating wheel, particularly illustrating the concept of front and rear 'jetting' and 'wake breathing'. These effects are described in more depth in Mears [10].

Saddlington et al. [11] combined published work of the flow field combined with their own LDA measurements to produce a comprehensive description of the downstream flow field. The concept of two large ground vortices or lobes with a central downwash and two smaller counter-rotating vortices on the tyre's upper shoulder was described. Knowles' conclusion (outlined in [11]) was that these vortices had rolled off the tyre's sidewall. As Fackrell's previous work also illustrated, the sidewall and profile as well as aspect ratio have a large effect on the aerodynamic characteristics of the wheel.

COOLING DRAG

Usually, cooling flows increase drag due to a proportion of the pre-entry streamtube momentum being lost at any one of the crucial stages (Seddon et al. [12]): the intake, cowl (friction drag from the surface), cooling or engine components' resistance and then most significantly, the exit (Barnard [13]). Flow approaching an inlet duct or scoop splits to follow one of two domains, the internal flow and the external flow. Generally, the design of an inlet is intended to carefully optimise the two flows in order to provide useful internal airflow combined with a minimal effect on the external flow and therefore the overall aerodynamic performance of the device.

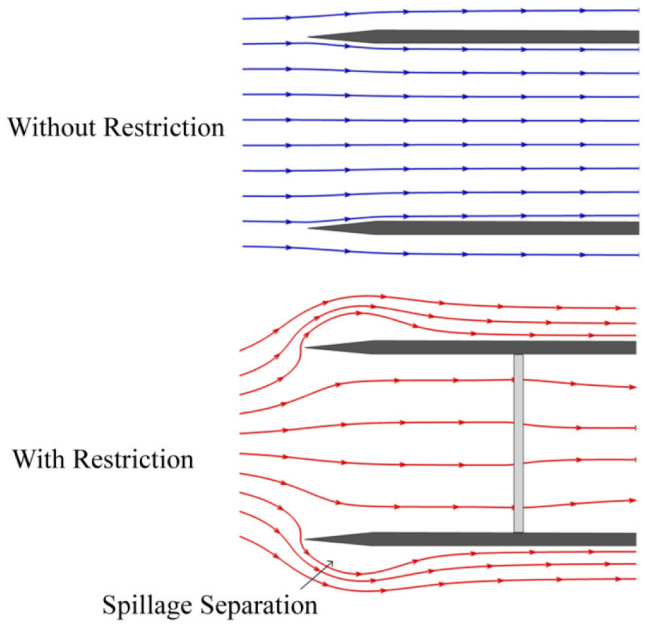

Figure 1. Illustrating the effect of introducing an intake restriction. Spillage separation is clearly shown in the lower part.

Typically, a study of through-body and cooling flows would illustrate the fact that increasing such flow will result in an increase in drag (Hucho [14]). An upper limit, named 'ram drag', seen in Equation 1, is often associated with cooling flows. This was found by Williams [15] to be an overstatement in the cooling drag penalty for production vehicles. Inlet spillage drag is an effect which is very prominent in aircraft inlet design, particularly at high subsonic and supersonic speeds where shocks are present (Seddon et al. [12]). It has not been extensively researched for low sub-sonic velocities. This process describes drag being induced by excess flow within the inlet capture streamtube which is being 'spilled' or diverted around the inlet without entering it (as in Figure 1). Lower or even negative cooling drag effects (Wiedemann [16]) are caused by this inlet spillage which is usually negligible in smooth or faired cases, where the streamtube's pre-entry momentum is fully recovered. Wiedemann also suggested a cooling flow dependent external yawed flow which increased the drag of the wheel as is consistent with the findings of Cogotti [17].

$$D_{ram} = \frac{1}{2}\rho_0 A_s V_s^2 \qquad (1)$$

Williams [15] produced an analytical formula, as shown in Equation 2, for predicting the contributions of the cooling drag. The initial term refers to the free stream momentum of the pre-entry streamtube. This momentum refers to the ram drag above and is essentially the drag from the internal flow. The second term is the contribution from the inlet on the external flow and the final term is the contribution from the

exit on the external flow. The inlet component (shown in Equation 3) comprises a thrust recovery coefficient which is unity when all pre-entry streamtube momentum is recovered and approaches zero when there is a complete energy loss. The assumption of this formula is that the inlet spillage drag effect disappears entirely once the through body flow equals that of the free stream. Figure 2 shows the form of the spillage drag with varying thrust coefficients.

$$\frac{\Delta D_{cooling}}{q_0 A_r} = \frac{\dot{m}_0 V_0}{q_0 A_r} + \frac{\Delta D_{spill}}{q_0 A_r} - \frac{(\dot{m}_6 V_6 \cos\alpha - \Delta D_{ub})}{q_0 A_r} \quad (2)$$

$$D_{spill} = \left(1 - c_{t,inlet}\right) q_0 A_s \left(1 - \frac{V_s}{V_\infty}\right)^2 \quad (3)$$

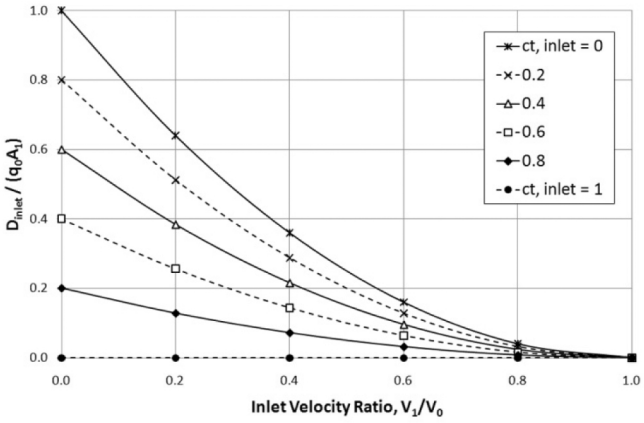

Figure 2. After Williams [15], illustrating the normalised drag contribution for varying velocity ratios and inlet thrust coefficients.

Few previous studies have investigated the effect of through-hub flow on a wheel's aerodynamic characteristics. In this study, a detailed investigation of through-hub flow is provided to build upon the now fairly well understood flow field of an isolated wheel. The aim of this investigation was to replicate, using realistic F1 geometries, a front wheel assembly including brake cooling channels and hub components to test varying levels of through-hub flow in order to investigate the relationship with drag and the form of the flow field and wake. Figure 3 illustrates a suggested internal hub-flow route.

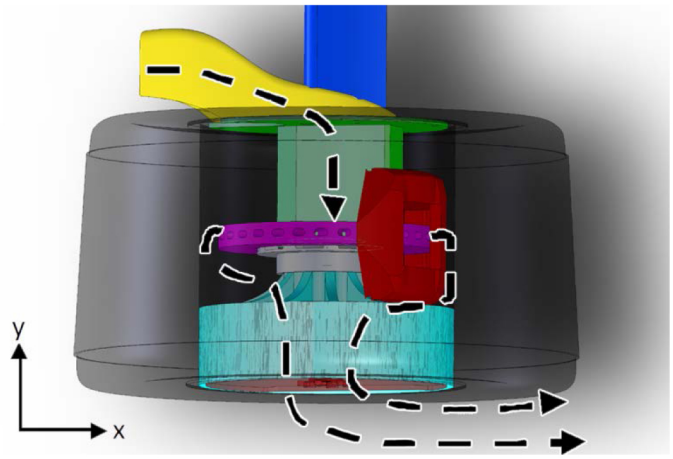

Figure 3. Common F1 front wheel assembly geometry and suggested through-hub flow pattern.

EXPERIMENTAL CONFIGURATION AND TECHNIQUES

WIND TUNNEL CONFIGURATION

A 50% scale Formula One front wheel assembly was tested in the Durham University 2m^2 open jet, open return wind tunnel. The wheel model being used generated a blockage of 3.66% including the sting arm and scoop and the tests were performed at a Reynolds number (based upon wheel diameter) of Re = 4.80×10^5 (in the supercritical regime, the importance of this was emphasised by Fackrell [4]). The tests were performed with a moving ground plane synchronised with the free stream velocity and full contact across the tyre's tread was ensured throughout. These data are consistent with accepted values for accurate wind tunnel testing of a rotating, exposed wheel.

The tyre used in this investigation was rigid in construction, made from carbon fibre and conical to allow tests at a camber angle of 3.5°, typical of a grand prix racing car front wheel. The tyre was mounted on an aluminium rim and attached to the hub assembly. A cross section of the assembly can be seen in Figure 4. The shrouding drum and brake scoop were produced by rapid prototyping techniques and were based on real F1 geometries. The tyre had an aspect ratio of 0.58, the dimensions of which conform to the FIA technical regulations for F1 and is comparable with the work of Fackrell [4].

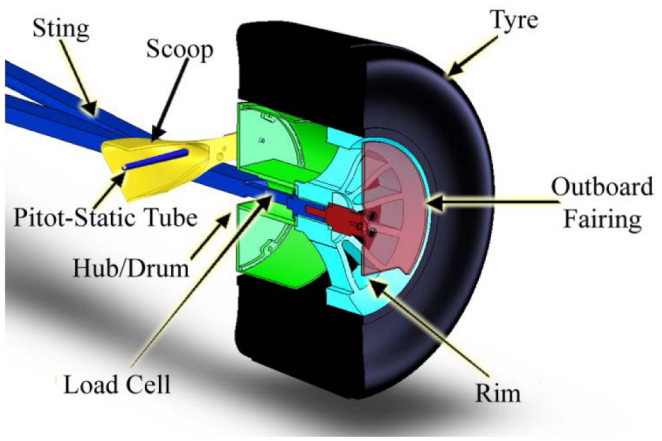

Figure 4. Centreline cut through of the wheel assembly (full scoop shown).

The intention was to investigate the effect of net through-hub flow and as a result the internal geometry was simplified. Instead of a brake disc, fine wire meshes were used at the interface between the scoop and the drum to vary the level of restriction (Figure 4). Common F1 practice is to intentionally design over sized brake ducts or scoops and then control the cooling flow at this interface depending on requirements of individual race circuits. Using meshes in this position allowed a range of through-hub flow conditions from fully closed (sealed) to fully open. In all cases, the scoop inlet area was left open so that any change on the external flow would purely be caused by the change in through-hub flow and not due to converting a scoop into a solid bluff body.

The drag measurements were performed using a strain gauge load cell situated within the hub (as shown in Figure 4). Each configuration was tested under two wind conditions. Firstly, a low speed tare was taken to account for bearing resistance which was considered velocity independent. This was performed at $1ms^{-1}$ with no wind ensuring negligible aerodynamic forces. This value was subtracted from the subsequent measurements which were performed at a velocity of $25ms^{-1}$. This way, the drag measurements calculated were purely the aerodynamic contributions. The voltages were recorded using a computerised data logger which recorded data for 65.5 seconds at 500Hz. The scoop velocities were measured by means of a pitot-static tube, made with rapid prototyping techniques and built into the scoop. This measured the velocity at the inlet cross section of the scoop where the flow was considered to be parallel to the freestream. These pressure measurements were recorded via the use of pressure transducers connected to the same data logger recording at the same frequency.

$$HFN = \frac{A_S V_S}{A_f V_\infty} \tag{4}$$

For scalability, the through-hub velocity was non-dimensionalised and termed the Hub Flow Number (HFN) defined by Equation 4. As there was an anticipated level of spillage from the open sided brake scoop, the flow velocity measured at the scoop would be larger than the through-hub velocity. A correction was formulated in order to convert scoop velocities into through-hub flow rates. This was done by using the CFD prediction (see later sub-section) to calculate the ratio between the scoop velocity and the through-hub velocity at the fully open case and for each scoop modification an empirical offset was measured for the closed case, as a closed intake could not possibly allow any through-hub flow. The correction is presented in Equation 5.

$$HFN_C = \frac{V_{s,CFD}}{V_{h,CFD}}(HFN - HFN_{closed}) \tag{5}$$

PRESSURE PROBE MEASUREMENT

Flow field data were measured at crossplane configurations (YZ) at 2D (two wheel diameters) downstream of the wheel's axle. This allowed an empirical measurement of the counter-rotating vortices under open and closed scoop conditions. The probe used was a five-hole configuration produced with rapid prototyping techniques and had a pitch and yaw sensitivity of ±40°. It was mounted on a slender mounting which in turn was connected to an automated three axis traverse unit built into the tunnel. These data were recorded at 800Hz for 2.56 seconds and with a grid spacing of 15mm in both directions resulting in a grid comprising 945 points.

PARTICLE IMAGE VELOCIMETRY (PIV)

The PIV was set up in two orientations referred to as longitudinal (XZ) planes and crossplanes (YZ) as defined by the axes in Figure 5. These were the most logical orientations in order to capture the motion of the flow around the wheel and through the hub. Two cameras (12 Bit Sensicam 1280×1024 with chip cooling) were mounted to take simultaneous instantaneous flow fields thus doubling the size of the captured image. The cameras were mounted on a one dimensional automated traverse unit and by traversing to four different locations downstream, a time-averaged flow field map could be produced which extended to 1.86D downstream of the axle. This region corresponded to the recirculation zones and flow field which were out of range for a five-hole pressure probe.

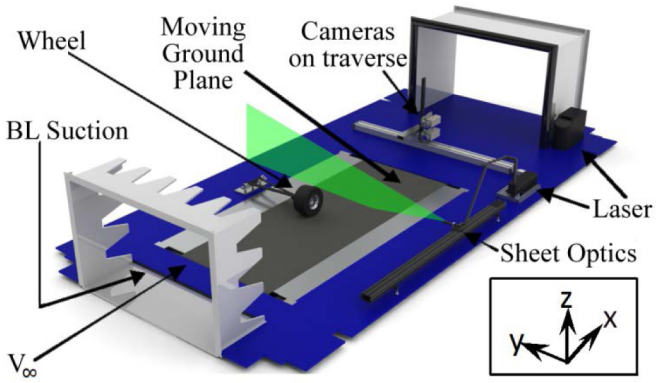

Figure 5. PIV Crossplane layout. XZ planes were performed by swapping the cameras and the laser sheet optics.

The flow was seeded by the use of a compressed air fed, 12 nozzle DEHS oil atomiser. This produced particle sizes of 1µm which are considered to follow the flow of the air without disturbing the measurements [18]. The seeding was injected into the airflow by means of a smoke rake positioned upstream of the nozzle contraction where it dispersed to the correct size by the model as well as providing minimal disruption to the airflow upstream of the model.

The crossplanes were constructed by similar means but with three camera locations instead of four, this time centred about the centreline of the wheel. Crossplane seeding was more complex than the former case as a volume rather than a plane needed to be filled with smoke. This was achieved by using four of the rakes previously used, side by side. PIV is challenging for crossplanes as the flow is almost entirely out of plane. Since the in-plane velocities were much smaller than in the XZ planes the timing had to be longer to ensure no signal drop out. It is a requirement to have a large enough separation time in order to allow significant particle movements between images (several pixels) but short enough to ensure the particles in both frames are the same ones in order to detect movements. An image separation of 25µs was used (compared to 15µs for the longitudinal case) which gave the best balance between allowing reasonable pixel movement and keeping the seeding within the flow. Since the particle movement was only of the order of one or two pixels, larger particles were a benefit. This is because Gaussian detection can be used in order to find the centre of a particle which is more than one pixel in diameter and therefore, to an extent, track sub-pixel movements. It was found that by defocusing the laser very slightly the particle sizes were increased at the cost of intensity. Moving the laser's focal length by around 150mm (over a focal length of 1.3m) caused an apparent particle size increase of 32% (2.2±0.1 to 2.9±0.1 pixels). This was assumed to be due to the slightly wider beam (in the process of converging or diverging) leading to a wider range of scattering angles from each particle, thus by the time the light reached the detector, the particle size was larger. This fact was considered in the setup of the crossplane measurements in order to ensure particle detection at such low in-plane velocities during short timescales. However, the sacrifice in intensity was sometimes detrimental so the level of defocusing used was judged and adjusted according to the image quality at the time.

The laser used was a class IV 120J double headed Nd:YAG cavity manufactured by New Wave Research. Beam delivery was achieved via an articulated arm attached to light sheet optics, optimised for the length scales involved in the size of tunnel being used. Ensuring a narrow beam with no clipping and as small a plane divergence angle as possible allowed the intensity to be maximised. The frequency of image pairs was set at 5Hz and 200 image pairs were collected in the case of the longitudinal planes. 300 image pairs were recorded for the crossplanes.

SURFACE FLOW VISUALISATION

The local flow around the scoop was investigated using surface flow visualisation techniques. A fluorescent powder was mixed with kerosene and spread evenly on the scoop surface which was subsequently placed in the airflow. The airflow evaporated the kerosene leaving a powder trace which displayed the flow field information on the surface. Subsequently, small black ink dots were placed on the surface in regions of interest. This was achieved using a hypodermic needle to ensure consistency of quantity and size. The test was run again which made apparent the forces and velocities as well as the direction which the initial fluorescent paint had shown. This was done for the open and closed scoop cases in order to see any dramatic changes in the airflow. The images produced were captured with a 6MP digital camera with UV lighting to provide greater contrast.

COMPUTATIONAL FLUID DYNAMICS (CFD)

Ansys Fluent was used with the Gambit mesh generation software to produce the domain. The high performance computing network was utilised which comprises a dedicated cluster of nodes with 802 processor cores available. The mesh contained 4.4 million cells and had a domain spanning 7D upstream of the wheel and 10D downstream with an area blockage of less than 4%. The mesh was tetrahedral with high detail in the hub section close to the tyre surface and scoop with lower resolution further away from the wheel. The interface between the scoop and hub plate was defined with a constant loss coefficient which was altered to match the experimental ranges. This allowed the required variation of through-hub flow to occur whilst keeping the external flow unaltered.

Various turbulence models were tested including the popular k-ε and k-ω models. The turbulence model used in this

publication was the single equation Spalart-Allmaras model (vorticity-based) which was least affected by late separation which leads to an unusually strong downwash. After some initialisation runs, 10,000 iterations were calculated with pressure, momentum and modified turbulent viscosity discretization solver options set at second order, QUICK and QUICK respectively. The tyre's surface was modelled as a static mesh but with moving surface conditions as was the floor. The spokes were defined by the gaps in between the metal and this was set as a rotating mesh centred on the axle rotating at the same rate and direction as the wheel.

RESULTS AND DISCUSSION

DRAG MEASUREMENTS

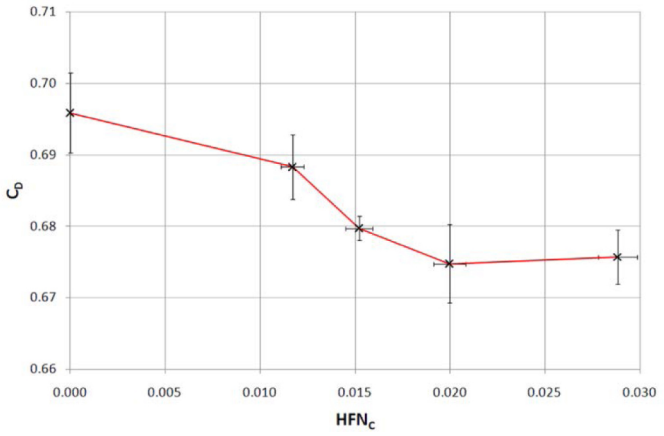

Figure 6. Drag Coefficient against Corrected Hub Flow Number for the unmodified scoop.

The results of the drag measurements for the unmodified scoop are shown in Figure 6. There exists a general decreasing trend in the drag coefficient with increasing hub flow number. There also exists a small increase toward the upper end of the hub-flow-number range. In all cases, the ram drag trend (velocity squared increase with hub-flow-number) is being dominated by another process which is also hub-flow-number dependent.

The concept of spillage drag has been applied in order to explain the reversal of the cooling drag trend. Equation 2 was used in order to predict the level of spillage drag for each case. This model already included the condition that the spillage drag effect tended toward zero as the through-body flow approached the free stream velocity and therefore, by setting a second condition for the zero hub-flow case, a value for $c_{t,inlet}$ could be calculated. As the theoretical increase in drag between the closed and open cases should equal the ram drag (Equation 1), the contribution of the spillage drag was assumed to be the ram drag plus the empirically measured difference between the two cases.

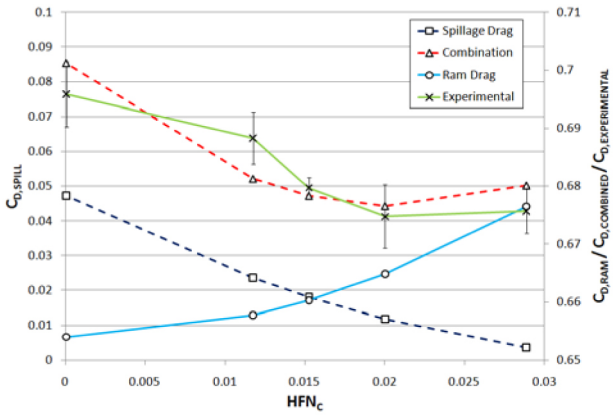

Figure 7. Combining the ram drag and spillage theory to produce a theoretical trend (triangular markers) compared with the experimental data for the standard scoop.

By combining the theoretical ram drag with the spillage to obtain a prediction of the measured drag as in Figure 7, one can see that the resulting trend strongly agrees with the experimental data. All but one point is within experimental error and it can be clearly seen that the effect of spillage drag trend dominates the ram drag prediction at low hub-flow-numbers.

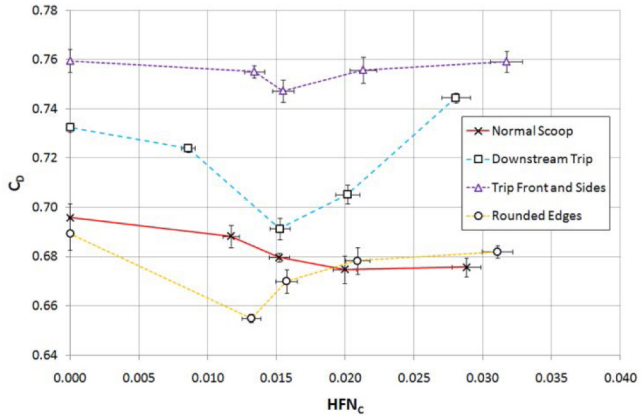

Figure 8. Drag Coefficient against Corrected Hub Flow Number for the configurations in Figure 4.

Four different scoop configurations were tested (Figure 8). These comprised the standard scoop design (as above), two modifications causing a deliberate separation to dominate any spillage drag effect which may have been present and one modification which rounded off the edges to produce a faired symmetrical aerofoil section at the leading edge (Figure 9). The latter was intended to reduce or eliminate the effect of spillage drag. The separation trips were intended to be used in order to confirm the spillage hypothesis, not to improve the airflow of the scoop. Each modification was tested at a range of different levels of through-hub restriction.

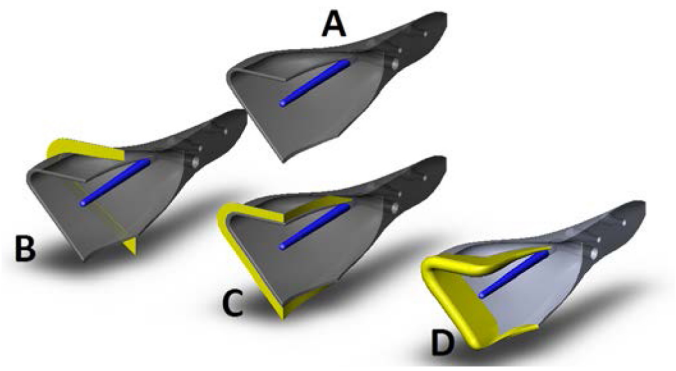

Figure 9. A - Normal scoop; B - Downstream separation trip; C - Separation trip at edges; D - Smoothed edges.

The first and obvious observation follows that the two cases with separation trips have a significantly higher drag coefficient compared to that of the unmodified scoop and the rounded edge modification. In both of the separation trip cases it can be seen that the overall drag trend results in a higher drag coefficient at higher hub-flow-numbers. However, all cases illustrate a reduction in drag followed by an increase, the severity and starting point of which is largely geometry dependent. It is clear to see that the smoothed leading edge case has a much lower drag coefficient for part of the range compared to that of the unmodified scoop. From Figure 8 it follows that larger spillage dominance would lead to a later rise in drag coefficient. This has been observed in the data where it can be seen that each of the modifications start the drag coefficient increase with an HFN_C around 0.015 compared to that of the unmodified case at 0.020. Table 1 shows the contribution of the spillage drag for each of the cases.

Table 1. Inlet thrust coefficients for scoop configurations, the maximum drag (closed scoop case) predicted by Williams' equation and the corresponding contribution to the overall wheel drag coefficient.

Configuration	$c_{t,inlet}$	D_{spill} (N)	$C_{D,spill}$
Normal	-0.186	1.075	0.047
Downstream Trip	0.340	0.650	0.029
Front and Side	-0.219	1.364	0.059
Smoothed Edges	0.104	0.891	0.039

The first observation is that some of these thrust coefficients are negative. This essentially describes a situation where Williams' model, under normal circumstances, under predicts the drag contribution from the spillage effect. As shown in Figure 2, a $c_{t,inlet}$ value of unity would imply the entire pre-entry streamtube momentum is recovered and therefore there is no contribution to drag from the inlet. By contrast, a value of zero would mean all of the momentum is lost and the maximum ram drag penalty is experienced at the inlet. A negative value would infer that there are further losses (similar to certain geometries which typically produce a drag coefficient greater than unity) which could be due to the fact that the separated flow may not have enough time to reattach before the end of the model and therefore contribute to a much larger separation of the overall wheel itself. This is discussed in depth in the later section on flow field studies. Essentially, the flow entering the scoop is flow which has already become separated and the more this flow is deviated from its path, the greater effect it will have on the overall model. This is why a stronger than normal spillage effect has been observed. Wiedemann [12] hinted at such a reversal of trends at high approach angles which is consistent with this explanation.

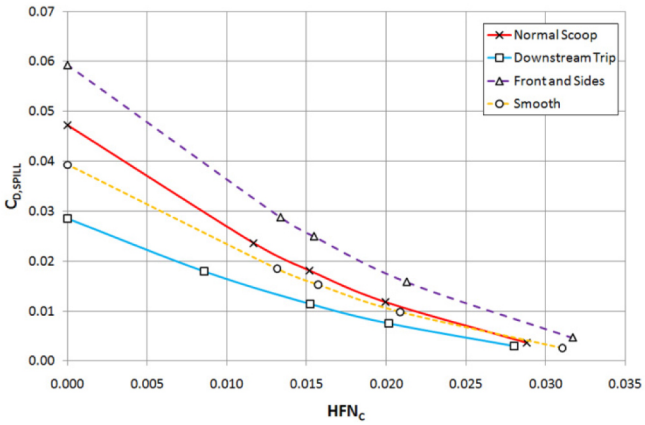

Figure 10. Spillage Drag Coefficient against Corrected Hub Flow Number for the configurations in Figure 4.

Figure 10 shows the calculated spillage contributions from the four cases. The case which illustrates the largest spillage contribution is the one with the front and side separation trips (Figure 9). This case was intended to simulate a large spillage effect over all through-hub velocities. Investigation of the surface flow field makes apparent the reasoning behind this result (later section). The case with the downstream separation trip has a drag contribution from the trip itself which makes this contribution closer to the order of magnitude of that of the spillage drag. Hence, a reduction in the contribution of the spillage drag is observed and a positive inlet thrust coefficient results. The majority of the drag influence from a free stream separation occurs (around half way down the scoop) where there is a perpendicular component to the face with respect to the free stream. Upwind of this, the scoop walls are parallel to the free stream so any separation would have minimal effect on the drag. The smoothed edge case has a small contribution from spillage drag using this model. Again, later discussions on the flow field across the scoop (rather than with the free stream) illustrates the key reason why spillage was reduced but not eliminated entirely. The model assumes the drag contribution from spillage reaches zero exactly as $Vs/V\infty = 1$ which is not what appears to be happening from Figure 8. By this, it

appears that the effect of spillage drag is eliminated entirely by the second point on the graph where it then begins to display the increasing trend.

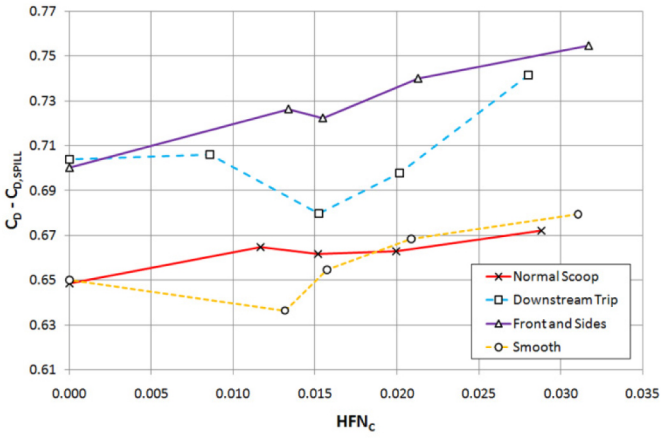

Figure 11. Corrected drag measurements with spillage component removed (Williams' model (Eq. 2)).

Figure 11 is a combination of the above results showing the raw drag measurements with the predicted inlet spillage effect removed. These graphs all show the expected upward trend with hub flow number. This suggests that the spillage drag explanation is consistent with the results. With the spillage effect removed, the form of the cooling drag appears to approximate a more linear relationship than velocity squared. However, given the number of influences on the cooling flow, this cannot be attributed to any one reason at this time.

FLOW STRUCTURE INVESTIGATION

Previous observations have made apparent that there are some interesting flow processes taking place in and around the scoop. To investigate this, a detailed investigation of the PIV, probe data, surface flow visualisation and CFD will now be discussed. For brevity, only the open and closed scoop interface cases will be considered to show the flow field at both extremes. An ‘open’ flow refers to the case where the scoop is open and maximum through-hub flow is allowed. Conversely, a ‘closed’ flow is one in which the scoop inlet interface has been sealed and hence no ducted air enters the hub.

SCOOP FLOW

It is apparent from the inboard planes that there is a horizontal ‘jet’ or interference which is present for the closed case but hardly noticeable for the open case. This coincides with the wheel's centre and more importantly, the scoop and the sting arm supporting the wheel. If one looks at the PIV stream traces in Figure 12 and the CFD in Figure 13 of flow over the scoop, it can be seen that the closed case causes spillage separation, not only over the leading edge of the scoop but more significantly over the upper and lower inside edges of the open sided scoop (solid white line in Figure 14). Causing a large separation here also influences the angle of incidence on the symmetrical aerofoil utilised for the sting which is intended to cause minimal resistance to the airflow. Conversely, for the open case, the spillage is smaller, although still present and therefore the air which approaches the sting is more suitable for the aerofoil section. The larger spillage separation for the closed case causes a steep incidence angle to the sting which is so severe that it causes a compounded effect on the wheel's overall flow by introducing a large separation region behind the sting. This is what is visible in the PIV planes, particularly the +70mm case. The open case has a smaller effect in both cases.

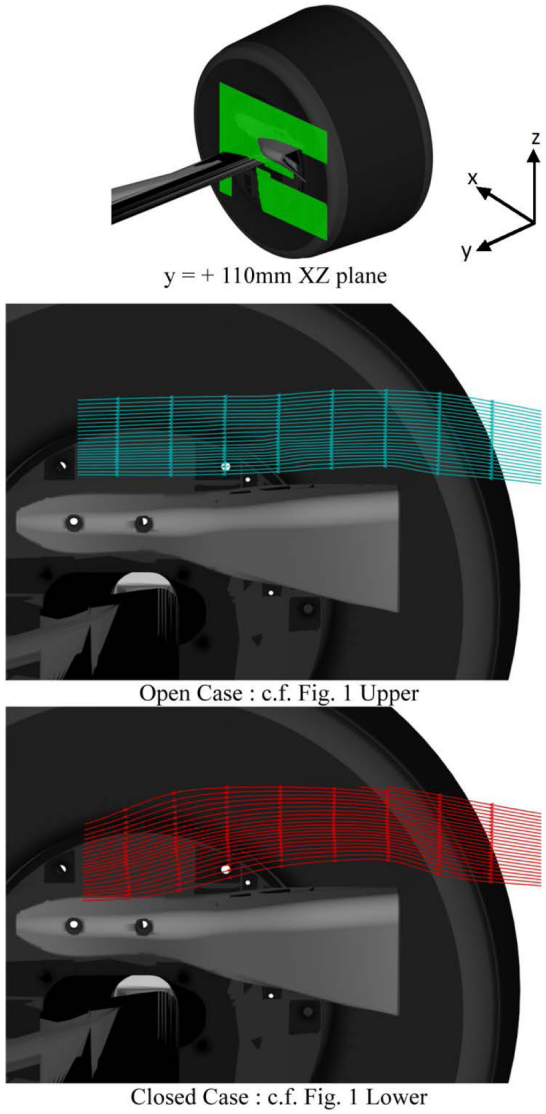

Figure 12. PIV flow field streamtraces over the scoop (based on in-plane velocity vectors). The flow in the closed case separates by a larger amount but reattaches converse to the open case.

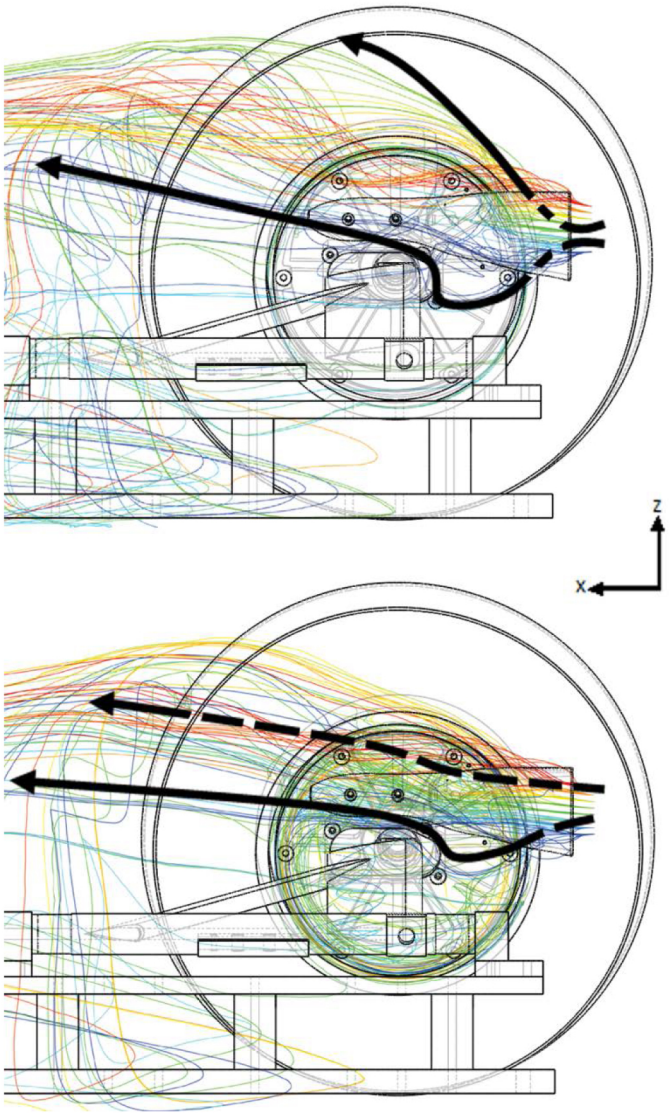

Figure 13. CFD streamtraces showing an array of points at the scoop entrance. Upper : Closed, Lower : Open. Streamtraces are not confined to X-Z plane so thick black lines have been used to illustrate the motion (dotted sections being flow travelling behind a solid surface).

Intricate details of the flow over the scoop suggest that it is a complex three dimensional flow. The surface flow visualisation studies, as in Figure 14, show some useful details of these. Dealing with the open case first, it appears that the flow is split into two main sections. To the left of the dotted line (region A) the flow has separated over the leading edge and upon reaching the dotted line, drops toward the surface and recirculates back to the leading edge. After this, the flow appears to follow the contours of the scoop as expected. There appears to be an element of spillage on the upper inner lip, the lower solid white edge of on the figure. This has caused a slight recirculation with the flow being directed back toward the inboard mounting plate. The pooling effect of the flow visualisation powder emphasises this.

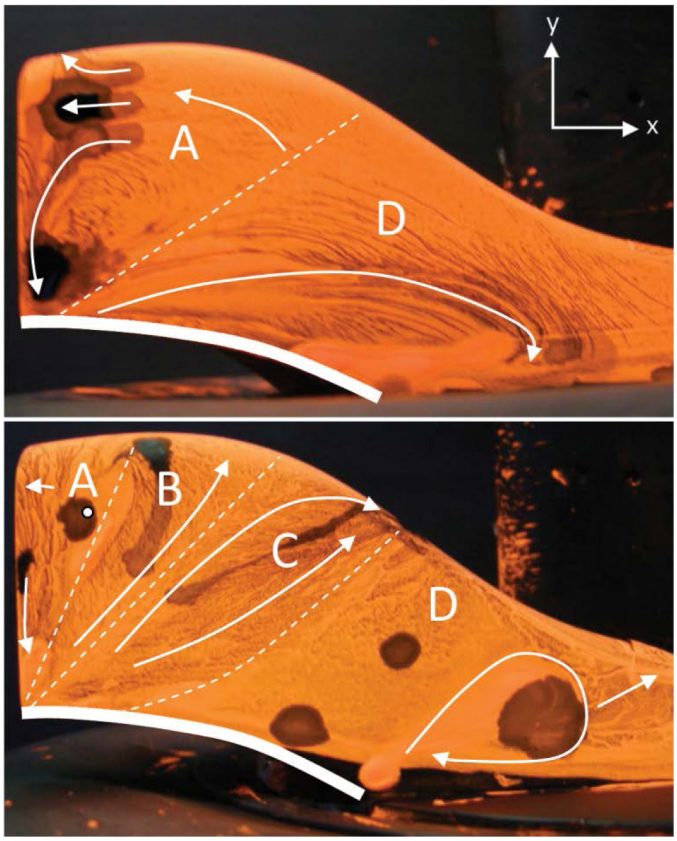

Figure 14. Scoop flow visualisation powder studies. Upper : Open scoop, Lower : Closed scoop.

The closed case appears to be a completely different flow structure with some unusual features. The flow can essentially be split into four different sections, separated by white dotted lines and labelled A, B, C and D. In section A there is a similarity to the flow over the open scoop case which shows an initial separation with a short recirculation bubble present, as confirmed by the detail in the PIV data in Figure 12. Region B occurs much earlier in the closed duct case and is brought about by the large spillage effect occurring from the inner lip (solid white line). There is a strong flow vector emanating from the front half of the solid white line (C) but as one moves closer to the blocked inlet the flow completely separates and gives rise to region D which has very little flow momentum at all. There is a pooling area of turbulent flow downstream of the interface with the inboard plate showing motion suggested by the white arrow. Again, the black dots provide contrast giving an idea of velocities and forces at work as well as the direction of motion.

The initial leading edge separation (XZ plane), with the flow of the free stream is larger on the open case. This is also evident in the PIV and CFD in Figures 12 and 13 respectively. Despite this, it is the large cross flow trend and

the separation under and over the scoop that causes the significant drag change measured in the closed case.

PIV - LONGITUDINAL (XZ) PLANES

Figure 15 (end of paper) shows the PIV measurements in the XZ plane, comparing the open and closed flow cases. Beginning with the centreline, there exists a large vertical downwash only present in this plane. This downwash turns against the free stream into the contact patch of the tyre. By looking at other planes closer to the side walls it is obvious that this downwash, in conjunction with edge effects of the low aspect ratio wheel, causes the large counter-rotating lobes as documented in Saddlington et al. [11]. The motion of the wheel's surface is not apparent in the PIV images due to a narrow shear layer which was undetected at this vector resolution. Essentially, the seeding within this region of flow which follows the wheel's rotation, due to the no slip condition, is overwhelmed at the analysis stage (due to the interrogation window size being larger than the shear layer) by the majority of the flow moving with the overall flow field. A similar observation can be made at the floor where the belt speed, equivalent to the free stream velocity is shown. It is believed that this has a larger shear layer than at the wheel surface and this is why it has been detected.

Comparing the open and closed flow cases, the first observation would be that the opening of the scoop causes a lower overall wake profile in all cases. This marginally lower turbulent region could be a partial reason for a lower than expected drag measurement for the open case. Further to this, it seems that the recirculation region, or ground lobe emanating from the wheel's contact patch, is made smaller on the inboard side and larger on the outboard side. This infers that allowing through-hub flow alters the entire structure of the wake by both changing the size and location of the trailing vortices.

CROSSPLANES

Figure 16 shows a subtraction of the closed from the open case for the PIV crossplanes taken close to the wheel's hub. As can be seen here, the open case seems to show larger ‘jetting’ at the ground level. There is also a visible and quantitative flow out of the hub at the axle level. This is due to the ducted flow through the hub.

When an inlet restriction is put in place, the flow through the hub would be dispersed over the whole spoke region, particularly in the case where a centrifugal flow brake disc is used as in McPhee et al. [19].

Investigation of the CFD shows some emphasised effects and a general over prediction of velocity vectors. However, the general structure is the same. It is very useful for understanding the general flow formation, particularly in regions in which the PIV cannot reach, such as inside the wheel. Figure 17 shows the crossplanes at 1D and Figure 18 shows them at 2D downstream highlighting the evolution of the counter rotating vortices. At 1D, the vortex structures are fairly tight and narrow with diameters of the order of 0.5D. There is also evidence, in the closed case, for an asymmetric flow. By opening the flow, the air is faster on the outboard side of the wheel and combined with a smaller turbulent region behind the sting this draws both vortex structures toward the centreline of the wheel. Each vortex is slightly larger, due to a faster central downwash and they are both comparable in size. Further downstream at 2D the vortices are much wider and lower with a larger separation between them. The in-plane vectors are around half of the magnitude they were at 1D suggesting the flow is beginning to recover from the wheel influence

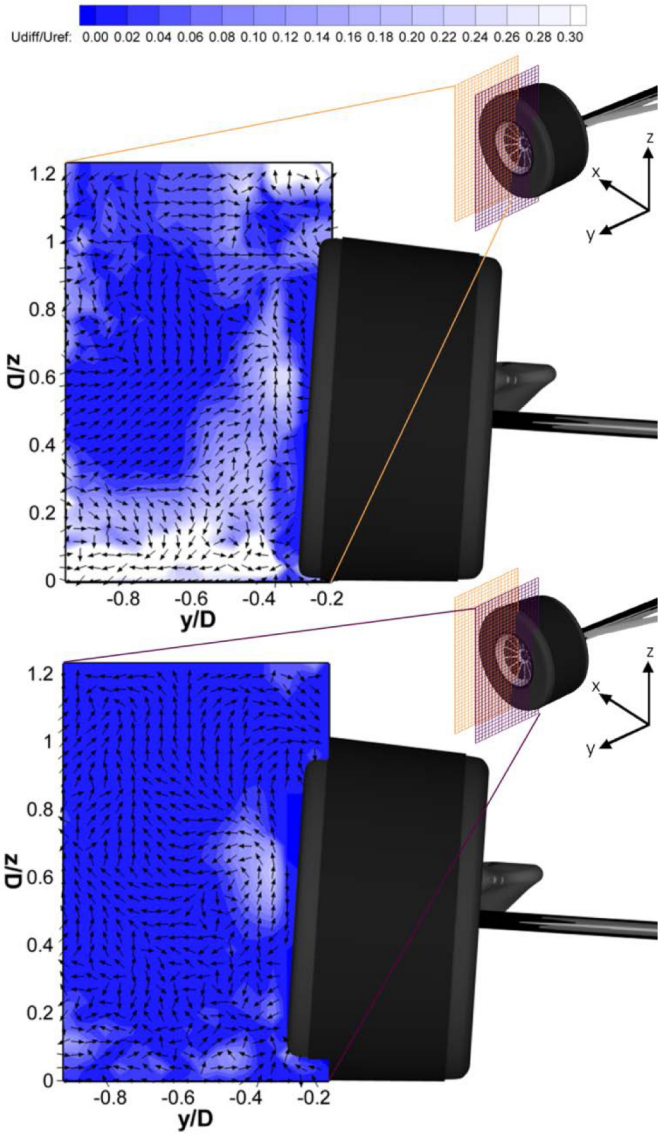

Figure 16. Difference plots (in-plane velocity) of the PIV crossplanes at x=0D (upper) and x=0.25D (lower).

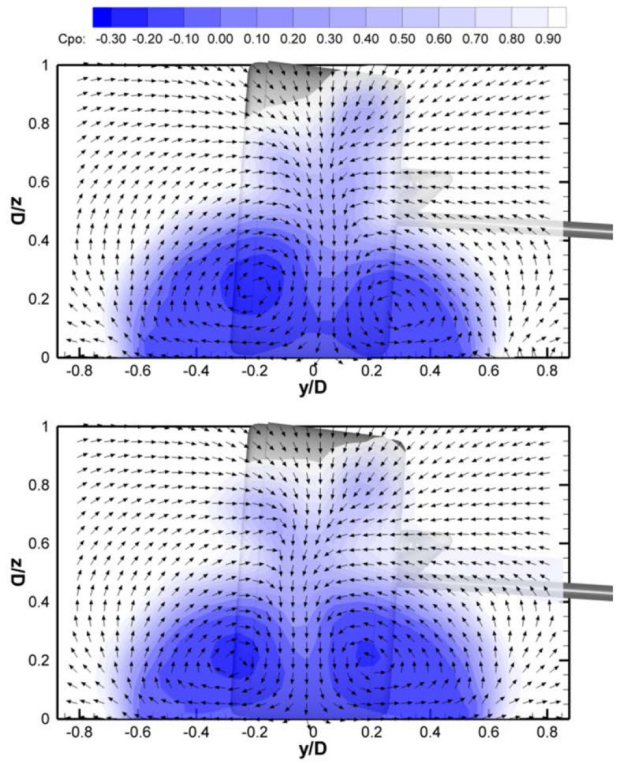

Figure 17. CFD Crossplane at 1D downstream showing in-plane velocities. Upper: Closed, Lower: Open.

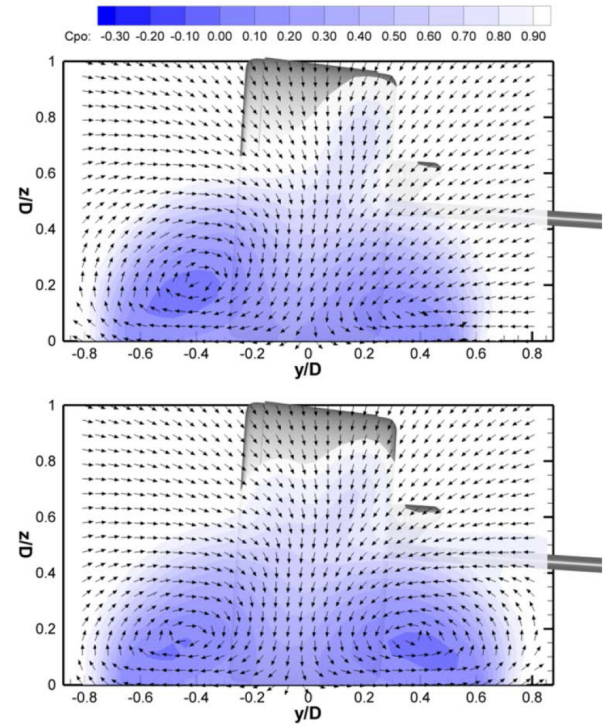

Figure 18. CFD Crossplane at 2D downstream showing in-plane velocities. Upper: Closed, Lower: Open.

OUTBOARD WHEEL COVER INVESTIGATION

As most of the literature points toward the exit flow being extremely important for through-body flows, the effects of outboard wheel fairings were investigated. A circular disc, the same diameter as the rim was constructed with a notched exit point based upon popular designs from the 2009 F1 season. Drag measurements were taken for four different locations of the exit. These were in the top, bottom, rear and forward facing directions. All other parts of this study were conducted without this fairing.

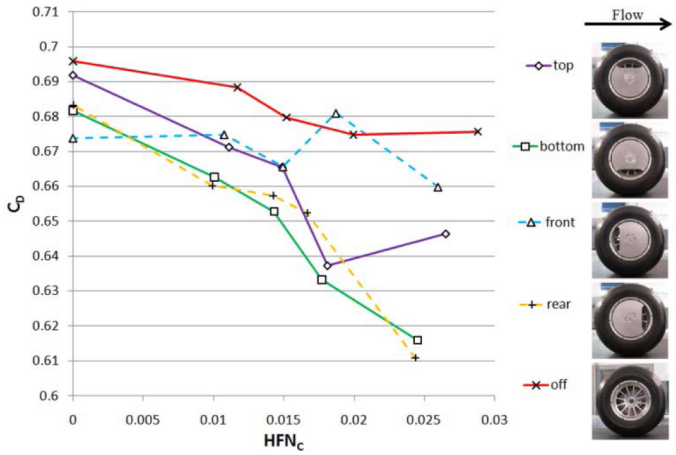

Figure 19. Drag Measurements of the outboard wheel fairing in different locations.

It is particularly interesting to note that, in previous years in F1, teams used now banned outboard wheel covers to aid the through-hub flow. By carefully directing the flow out of the hub the location of the point where the exit momentum can be controlled and therefore influence the overall wake of the wheel. Figure 19 shows the drag measurements for the outboard plate used in this part of the experiment. The open flow case is the most susceptible to exit flow conditions as it is not dispersed and therefore the jet flowing through the hub will be heavily affected by the location of the exit orifice. The two cases with the exit orifice in the lower and rearward pointing positions cause significantly less drag than the other cases. By facing the exit orifice toward the front of the wheel, the through-hub flow must undergo a complete change in direction, similar to a turning vane or exit flow which is at a different angle to the inlet on an Ahmed model [13]. The lower sidewall is the source of the majority of the wake and as Figure 16 showed, there is a strong flow at ground level, the height of the sidewall of the tyre, flowing in the direction of the through-hub flow (due to jetting and separation from the frontal contact patch). Because of these observed features, more momentum recovery can take place here than the upward pointing case and hence an explanation for reduced drag. This suggests that the way in which the through-hub

flow is reintroduced into the global flow is of highest importance for high flow rates.

FIVE-HOLE PROBE WAKE MAPS

The wake maps shown in Figure 20 show the counter rotating vortices favouring the outboard side with a through-hub flow compared to the case of no through-hub flow. The lower part of the figure also shows the wake structure with the outboard hub plate in position (downward facing). This shows a stronger effect of the same trend. This implies that focusing or directing the flow out of the hub not only reduces the drag but also moves the wake toward the outboard side. F1 aerodynamics in particular are highly sensitive to the state of the air immediately behind the front wheel suspension and leading into the side pods and underfloor. Moving the inboard trailing vortex further outboard could be beneficial in terms of optimising the state of the airflow leading to those downstream components and hence, increasing through-hub flow has a much more influential effect on F1 aerodynamics than the primary purpose of brake cooling.

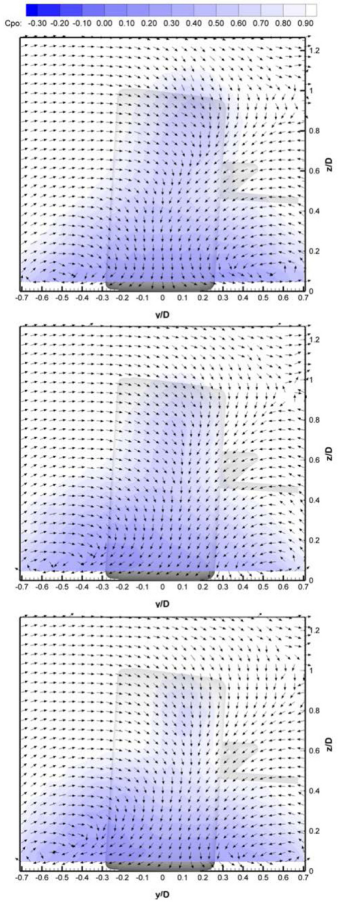

Figure 20. Probe wake map of the crossplane at 2D downstream showing in-plane velocities. Upper: Closed, Middle: Open, Lower: Open with downward facing hub fairing.

CONCLUSIONS

An investigation into the effect of through-hub flow on a 50% scale F1 wheel assembly was considered and tested in the Durham University 2m^2 wind tunnel. PIV, five-hole pressure probe measurements and CFD were utilised in order to investigate the flow field in and around the wheel and flow visualisation techniques were used to obtain surface effects. Drag measurements were obtained at varying through-hub flow rates which were measured using a pitot-static tube situated in the entry of the brake scoop.

The effect of through-hub flow on a rotating exposed wheel is not an insignificant one. Studies of drag measurements for varying levels of through-hub flow show a negative cooling drag effect whereby the drag increases with the reduction of internal flow rate. This effect had been hinted at by Williams [15] and Wiedemann [16]. Inlet spillage has been identified as the primary reason for these observations. By closing the inlet orifice at the interface between the open sided brake scoop and hub assembly, the excess airflow undergoes an extreme deviation around the outer edges of the scoop causing an excessive separation region. This effect is primarily noticed on the inner edges of the scoop, close to the tyre's side walls. Due to this, the flow field around the inlet scoop is far different in the open and closed cases with a high transverse velocity component in the closed case.

This separation region in itself can be linked to higher drag but upon closer inspection (Figure 13) there is a clear interaction with the flow field around the support sting which was located on the inboard side in place of the real vehicle's suspension geometry. In the closed scoop case, the attack angle on the wheel sting becomes extreme close to the wheel and causes a large separation. Although any drag on the sting would not be measured using the techniques employed here with a load cell placed inside the hub, the effect on the overall flow field of the wheel is not insignificant and could therefore have further effects on the overall wheel's drag. As the reality of F1 front suspension geometry is far more complex with several arms originating from the main body of the vehicle to form the uprights, damper arms and steering rods, this observation would be worth investigating further.

Several modifications were applied to the brake scoop in order to minimise or overwhelm the effect of this spillage drag in order to confirm this explanation in terms of drag measurement trends. An extension to the scoop's edges was added with the intention of deliberately causing separation at all times thus eliminating the spillage separation condition. Although this did not reverse the trend entirely, the effect of spillage drag became less significant and the higher flow rates resumed the usual increase in drag with cooling flow as expected. Likewise, rounding off the edges of the leading and inside edges resulted in a slight reduction in the spillage drag component, although from the CFD and surface effects

(Figure 14) it is evident that the large crossflow separation cannot be reattached by such means. The rounded edges did, however, reduce the overall drag of the device and therefore improved the aerodynamic efficiency. It would suggest that by doing this, the separation region in region A (Figure 14) would be reduced or even eliminated and therefore simplify the flow.

By applying the prediction formulae of Williams' [15] in order to estimate the effect of the inlet and exit flow drag components, the argument is reinforced by reversing the trend and displaying a drag curve closer to that which would be expected (as in Wiedemann [16]). It is therefore an important conclusion that the usual ram drag expression (Equation 1) is inappropriate for such complex flows where there are high angles of attack or where the device in question is already in a separated region.

Exit flows are considered to be of utmost importance with cooling or internal body flows ([12,13]) and observations in this investigation are no different. Sensitivity to the open case is present in the outboard hub cover experiment which shows very different trends for different exit flow conditions. Outboard covers or fairings are documented to reduce the overall drag of the vehicle (Dimitrion et al. [20]) but again, there is little or no published work referring to an opening in such devices investigating through-hub flow. It was found that positioning the exit orifice at the bottom or facing rearward was the most beneficial to the overall drag due to the way the through-hub flow was reintroduced into the wheel's wake.

Investigations of crossplanes show the two counter rotating vortices as expected and changing the through-hub flow changes the entire structure of these. It is apparent that opening the through-hub flow allows the vortices to become symmetrical although slightly larger in size. This again could be due to beneficial changes to the inboard side as well as the flow jetting out from the outboard side of the wheel. Benefits of moving the inboard vortex toward the outboard side may include ‘cleaner air’ being fed into the underfloor components and side pods as well as potentially having smaller barge boards to deal with such disruption behind the wheel.

In conclusion, the brake cooling system of an F1 (or similar) front wheel results in a complex flow structure which has a considerable effect on the overall wake of the wheel as well as on the aerodynamic efficiency. Increasing the through-hub flow rate results in a decrease in drag and an increase in the size of the now symmetrical counter rotating vortices. The spillage separation from the upper and lower internal sides of the open ended scoop cause interference with other devices on the vehicle. The effect in this experiment was to the detriment of the flow structure due to interference with the support arm. On a current F1 car this could be used to benefit the efficiency of the overall vehicle despite the loss in efficiency of the wheel. For example, the downward spilled flow from the scoop could be directed under the car for increased downforce in this region. Control of the through-hub flow is therefore vital in terms of the wake downstream interfering with the side pods and ultimately the rear tyres, rear wing and diffuser. The flow around the scoop and its effect on the suspension arms, the underbody of the car and the internal flow itself in terms of brake cooling efficiency are also of primary concern.

REFERENCES

1. Dominy, R. G., Aerodynamics of Grand Prix Cars. Proc. Instn Mech. Engrs. Part D, 206D, pp267-274, 1992.

2. Fackrell, J. E. and Harvey, J. K., The Flow Field and Pressure Distribution of an Isolated Road Wheel, Advances in Road Vehicle Aerodynamics. BHRA Fluid Engineering Conference - Paper 10, 1973.

3. Fackrell, J. E. and Harvey, J. K., The Aerodynamics of an Isolated Road Wheel. Proceedings of the Second AIAA Symposium of Aerodynamics of Sports and Competition Automobiles, Vol. 16, 1975.

4. Fackrell, J. E., The Aerodynamics of an Isolated Wheel Rotating in Contact with the Ground. PhD Thesis, University of London. 1974.

5. Morelli, A., Aerodynamic Effects on an Automobile Wheel. Technical Report Trans. 47/69, MIRA, 1969.

6. Stapleford, W. R. and Carr, G. W., Aerodynamic Characteristics of Exposed Rotating Wheels. Technical Report 1970/2, MIRA, 1970.

7. Mears, A., Dominy, R., and Sims-Williams, D., “The Air Flow About an Exposed Racing Wheel,” SAE Technical Paper 2002-01-3290, 2002, doi:10.4271/2002-01-3290.

8. Mears, A., Crossland, S., and Dominy, R., “An Investigation into the Flow-Field About an Exposed Racing Wheel,” SAE Technical Paper 2004-01-0446, 2004, doi: 10.4271/2004-01-0446.

9. Mears, A. P., Dominy, R. G., Sims-Williams, D. B., The Flow About an Isolated Rotating Wheel - Effects of Yaw on Lift, Drag and Flow Structure, 4th MIRA Int. Vehicle Aerodynamics Conf., Warwick, UK, October 2002.

10. Mears, A. P., The Aerodynamic Characteristics of an Exposed Racing Car Wheel. PhD Thesis, University of Durham, 2004.

11. Saddlington, A. J., Knowles, R. D., Knowles, K., Laser Doppler Anemometry Measurements in the Near-Wake of an Isolated Formula One Wheel, Springer-Verlag, Exp. Fluids 42:671-681, 2007.

12. Seddon, J. and Goldsmith, E. L., Intake Aerodynamics, AIAA Education Series, pp217-220, 1985.

13. Barnard, R. H., Theoretical and Experimental Investigation of the Aerodynamic Drag due to Automotive Cooling Systems, Proc. Instn Mech. Engrs. Vol. 214 Part D, 2000.

14. Hucho, W.H., "Aerodynamics of Road Vehicles 4th Edition," SAE International, Warrendale, PA ISBN: 978-0-7680-0029-0, 1998, doi:10.4271/R-177.

15. Williams, J., "Aerodynamic Drag of Engine-Cooling Airflow With External Interference," SAE Technical Paper 2003-01-0996, 2003, doi:10.4271/2003-01-0996.

16. Wiedemann, J., "The Influence of Ground Simulation and Wheel Rotation on Aerodynamic Drag Optimization - Potential for Reducing Fuel Consumption," SAE Technical Paper 960672, 1996, doi: 10.4271/960672.

17. Cogotti, A., Aerodynamic Characteristics of Car Wheels, International Journal of Vehicle Design, SP3:1983-173-196, 1983.

18. Riethmuller, M. L., Particle Image Velocimetry, Lecture Series, von Karman Institute for Fluid Dynamics, p49, 1996.

19. McPhee, A. D. and Johnson, D. A., Experimental Heat Transfer and Flow Analysis of a Vented Brake Rotor, International Journal of Thermal Sciences 47, pp458-567, 2008.

20. Dimitriou, I. and Klussmann, S., "Aerodynamic Forces of Exposed and Enclosed Rotating Wheels as an Example of the Synergy in the Development of Racing and Passenger Cars," SAE Technical Paper 2006-01-0805, 2006, doi: 10.4271/2006-01-0805.

CONTACT INFORMATION

Mr. Adam Sprot
a.j.sprot@durham.ac.uk
Durham University
School of Engineering and Computing Sciences
South Road, Durham DH1 3LE. U.K.

ACKNOWLEDGMENTS

The authors of this publication would like to express their thanks to Red Bull Technology for their support in this investigation. Thanks also go to Jack Williams for useful discussions relating to inlet spillage drag and Michael Wilson for discussions relating to F1 through-hub flow processes.

DEFINITIONS/ABBREVIATIONS

HFN
Hub Flow Number

HFN_C
Corrected Hub Flow Number

DEHS
Di-ethyl Hexyl Sebacate

D
Wheel Diameter

α
Exit flow inclination angle

q_0
Free stream dynamic pressure

D_{ram}
Ram drag force

$D_{cooling}$
Cooling Drag

D_{spill}
Inlet drag force (spillage)

D_{ub}
Underbody drag (not relevant for this study)

$\dot{m}_0$
Free stream mass flow rate

$\dot{m}_6$
Exit mass flow rate

C_D
Drag Coefficient

$c_{t,inlet}$
Inlet thrust coefficient

Cp_O
Stagnation Pressure Coefficient

ρ_0
Air density

A_r, A_s
Scoop area

A_f

Frontal model area

V_0, V_∞, U_{ref}

Free stream velocity

V_s

Scoop velocity

$V_{s,CFD}$

CFD Scoop velocity prediction

$V_{h,CFD}$

CFD Hub velocity prediction

V_6

Exit flow velocity

U

Local in-plane velocity

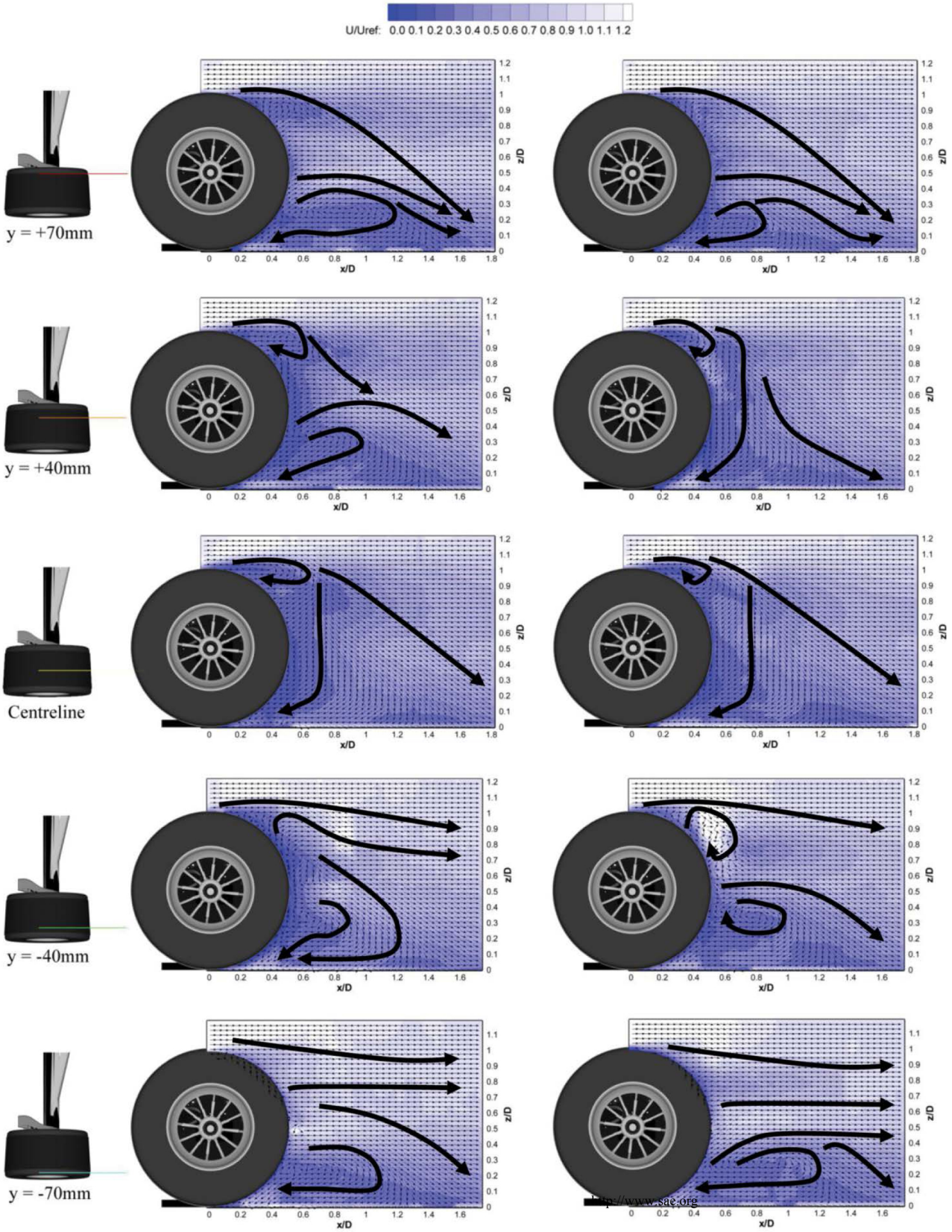

Figure 15. PIV longitudinal planes. Left : Closed, Right : Open. All velocities are in-plane components of the flow field. The thick black lines are to illustrate features of the flow shown by the velocity vectors and are not to scale.

The Engineering Meetings Board has approved this paper for publication. It has successfully completed SAE's peer review process under the supervision of the session organizer. This process requires a minimum of three (3) reviews by industry experts.

ISSN 0148-7191

SAE Customer Service:
Tel: 877-606-7323 (inside USA and Canada)
Tel: 724-776-4970 (outside USA)
Fax: 724-776-0790
Email: CustomerService@sae.org
SAE Web Address: http://www.sae.org
Printed in USA